Structural Engineering and Mechanics, *Vol. 51, No. 6 (2014) 1067-1089*
DOI: http://dx.doi.org/10.12989/sem.2014.51.6.1067

Three dimensional static and dynamic analysis of two dimensional functionally graded annular sector plates

Kamran Asemi, Manouchehr Salehi* and Mojtaba Sadighi

Mechanical Engineering Department, Amirkabir University of Technology, Tehran, Iran

(Received September 15, 2012, Revised May 6, 2014, Accepted July 20, 2014)

Abstract. In this paper, three dimensional static and dynamic analyses of two dimensional functionally graded annular sector plates have been investigated. The material properties vary through both the radial and axial directions continuously. Graded finite element and Newmark direct integration methods have been used to solve the 3D-elasticity equations in time and space domains. The effects of power law exponents and different boundary conditions on the behavior of FGM annular sector plate have been investigated. Results show that using 2D-FGMs and graded elements have superiority over the homogenous elements and 1D-FGMs. The model has been compared with the result of a 1D-FGM annular sector plate and it shows good agreement.

Keywords: three dimensional elasticity; graded finite element method; 2D-FGM annular sector plate; static and dynamic analysis

1. Introduction

Functionally graded materials (FGMs) are composite materials that are microscopically inhomogeneous, and the material properties vary continuously throughout the structure. This is obtained by gradually changing the composition of the constituent materials along one or more direction. Advantages of FGMs over laminated composites are eliminating the delamination mode of failure, reducing thermal stresses, residual stresses and stress concentration factors. Therefore, FGMs can be tailored to satisfy different requirements for material service performance at different parts or locations in a structure. The annular sector plates are widely employed as a part of engineering structures, including civil, mechanical, and aerospace engineering. Therefore, it is important to study the behavior of annular sector plates made of FGMs for the technical design of these structural elements.

Many studies have been performed to analyze the static and dynamic behavior of FGM structures (Asemi *et al*. 2010, 2011, Rahmati Nezhad *et al*. 2011, Ghannad *et al*. 2012, Yas *et al*. 2011, Behravan Rad 2012, Bian and Wang 2013). Among the FGM plate structures, little attention has been given to static and dynamic analysis of FGM annular sector plates. For example, Nosier and Fallah (2008) based on the first-order shear deformation plate theory obtained analytical solutions for axisymmetric and asymmetric behavior of FGM circular plates with various clamped

*Corresponding author, Associate Professor, E-mail: msalehi@aut.ac.ir

http://www.techno-press.org/?journal=sem&subpage=8 ISSN: 1225-4568 (Print), 1598-6217 (Online)

and simply supported boundary conditions under mechanical and thermal loadings. Li *et al*. (2008) using a direct displacement method analytically solved the axisymmetric problem of FGM annular plate subject to a uniform transverse load. Sburlati and Bardella (2011) obtained three-dimensional elastic solutions for FGM thick circular plates subjected to axisymmetric conditions. They utilized a Plevako's representation form which reduces the problem to the construction of a potential function satisfying a linear fourth-order partial differential equation. Lei and Zheng (2009) presented an exact analysis for axisymmetric bending of FGM circular plate. The displacement function was expanded as Fourier-Bessel series. Reddy *et al*. (1999) studied axisymmetric bending and stretching of FGM solid and annular circular plates using the first-order shear deformation Mindlin plate theory. Li *et al*. (2006) investigated the pure bending problem of simply supported transversely isotropic circular plates. They derived the stress functions for the axisymmetric deformation problem. Also, they investigated the bending of transversely isotropic circular plates subject to a transverse load in the form of qr^k (Li *et al*. 2008). They presented analytical elasticity solutions for simply-supported and clamped plates. Aghdam *et al*. (2010) presented an iterative procedure based on the First Order Shear Deformation Theory and the extended Kantorovich method (EKM) to gain highly accurate solution for bending of moderately thick FG fully clamped sector plates. Using the direct displacement method, Yun *et al*. (2010) investigated the axisymmetric bending of transversely isotropic and FG circular plates subject to arbitrarily transverse loads. The transverse load was expanded in the Fourier-Bessel series and superposition principle was used to obtain the total response based on the results of each item of the series.

The above literature review denotes that the dynamic analysis of FGM annular sector plates has been given little attention by the research groups. However, some studies have been done on free vibration of FG annular and annular sector plates (Saidi *et al*. 2011, Tajeddini *et al*. 2011, Jodaei *et al*. 2012, Dong 2008, Nie and Zhong 2008, Tahouneh and Yas 2012).

In the above mentioned papers, the material properties are assumed having a smooth variation usually in one direction. Due to difficulty in obtaining analytical solutions for dynamic response of graded material systems, analytical or semi-analytical solutions are available only through a number of problems with simple boundary conditions, i.e., for annular sector plates with simply supported radial edges (Saidi *et al*. 2011,Tahouneh and Yas 2012, Nie and Zhong 2008). Therefore, powerful numerical methods are needed to solve the governing equations. The graded finite element method (GFEM) is a relatively new numerical technique in structural analysis. This method incorporates the material property gradient at the size scale of the element and employs a generalized isoparametric formulation. Some works can be found in the literature on modeling non-homogenous structures by using GFEM (Santare *et al*. 2003, Kim and Paulino 2002, Santare and Lambros 2000, Zhang and Paulino 2007, Asgari *et al*. 2009, 2010, 2011, Asemi *et al*. 2011, 2012). In these researches, it is shown that the conventional FEM formulation cause a discontinuous stress field in the direction perpendicular to the material property gradation, while the graded elements give a continuous and smooth variation. However, when the loading is parallel to the material gradation direction, the GFEM formulation estimates sharp jumps in stress at the element boundaries while the conventional FEM formulation does not. The use of a GFEM has several benefits over the use of conventional FEM in the dynamic and wave propagation analyses. In conventional FEM, the boundary of homogenous elements of an inhomogeneous material acts as discrete boundaries for the stress waves. These boundaries cause artificial wave reflections and have a cumulative effect on the magnitude and speed of propagating stress waves. In addition, these inaccuracies will be more significant in 2D-FGM problems. Therefore, by using GFEM in which the material property is graded continuously through the elements, accuracy can

be improved without refining the mesh size.

Conventional FGMs may also not be so effective in such design problems since all outer surface of the body will have the same composition distribution. Therefore, variation of volume fraction in two directions has a higher capability to reduce the mechanical, thermal and residual stresses and leads to a flexible design than 1D FGMs. Some studies have been carried out about static, dynamic and free vibration of structures made of 2D-FGMs (Goupee 2006, Nemat-Alla 2009, Sobhani Aragh and Hedayati 2012, Shariyat and Alipour 2011, Nie and Zhong 2007, Lu *et al*. 2008, Behravan Rad and Shariyat 2013).

The main aim of the present paper is to present static and dynamic analyses of 2D-FGM annular sector plate based on three dimensional theory of elasticity. Material properties vary through both the radial and axial directions continuously. To solve the problem, graded finite element method and Newmark direct integration method have been applied. Using this method, discontinuities and inaccuracies which could be produced in the conventional FEM has been improved. Using this method, the effects of power law exponents and different boundary conditions on distribution of displacements and stresses have been investigated.

2. Governing equations

A functionally graded annular sector plate with thickness h, inner radii a and outer radii b is considered. The plate is subjected to a distributed load p on its top surface. The geometry and coordinate system of the plate is shown in Fig. 1.

Two-dimensional FGMs are usually made by continuous gradation of three or four different material phases where one or two of them are ceramics and the others are metal alloy phases, and the volume fractions of the constituent materials vary continuously through the r and z directions in a predetermined composition profile. The inner surface of the plate is made of two distinct ceramics and the outer surface of two metals. c_1, c_2, m_1 and m_2 denote first ceramic, second ceramic, first metal and second metal, respectively. The volume fraction distribution function of

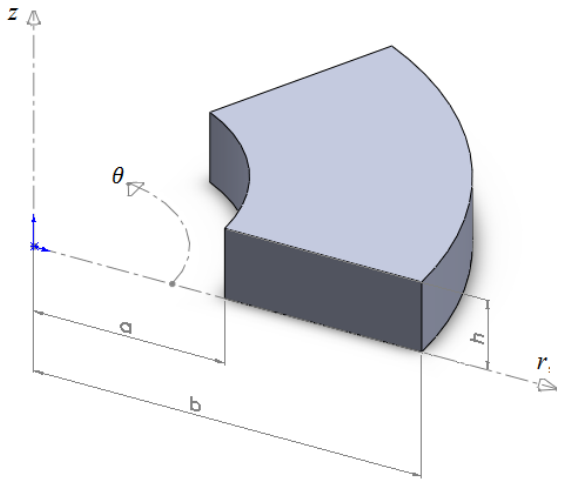

Fig. 1 Geometry of annular sector plate

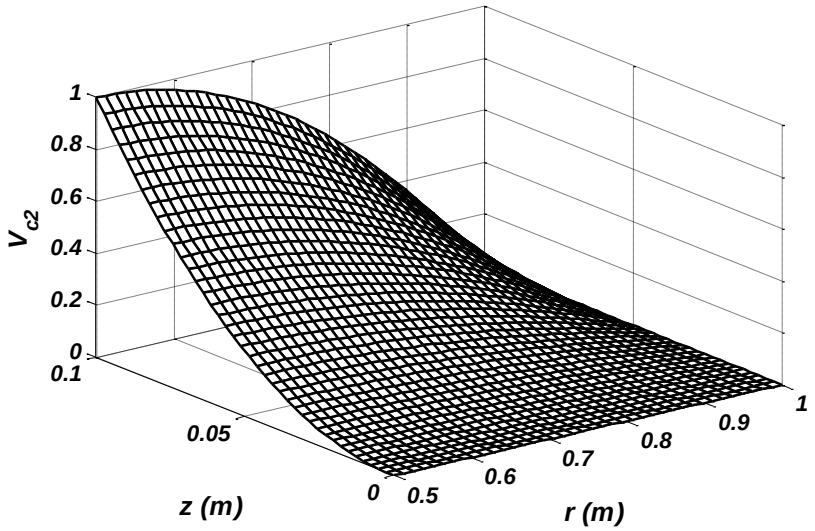

Fig. 2 Volume fraction of second ceramic for n_r=2, n_z=3

each material can be expressed as (Asgari and Akhlaghi 2009)

$$Vc_1 = \left(1-\left(\frac{r-a}{b-a}\right)^{n_r}\right)\left(1-\left(\frac{z}{h}\right)^{n_z}\right) \tag{1-1}$$

$$Vc_2 = \left(1-\left(\frac{r-a}{b-a}\right)^{n_r}\right)\left(\frac{z}{h}\right)^{n_z} \tag{1-2}$$

$$Vm_1 = \left(\frac{r-a}{b-a}\right)^{n_r}\left(1-\left(\frac{z}{h}\right)^{n_z}\right) \tag{1-3}$$

$$Vm_2 = \left(\frac{r-a}{b-a}\right)^{n_r}\left(\frac{z}{h}\right)^{n_z} \tag{1-4}$$

Where n_r and n_z are non-negative volume fraction exponents through the r and z directions. For instance, the volume fraction distribution of second ceramic for the typical values of n_r=2, n_z=3 is shown in Fig. 2. In this case h=0.1 m, a=0.5 m and b=1 m.

Material properties at each point can be obtained by using the linear rule of mixtures. Therefore, the material property P such as modulus of elasticity and mass density in the 2D-FGM annular sector plate is determined by linear combination of volume fractions and material properties of the basic materials as (Asgari and Akhlaghi 2009)

$$P = Pc_1Vc_1 + Pc_2Vc_2 + Pm_1Vm_1 + Pm_2Vm_2 \tag{2}$$

Table 1 Basic constituents of 2D-FGM annular sector plate (Asgari and Akhlaghi 2009)

Constituent	Material	E (GPa)	$\rho(\frac{Kg}{m^3})$
m_1	Ti6A14V	115	4515
m_2	A1 1,100	69	2715
c_1	SiC	440	3210
c_2	A12O3	300	3470

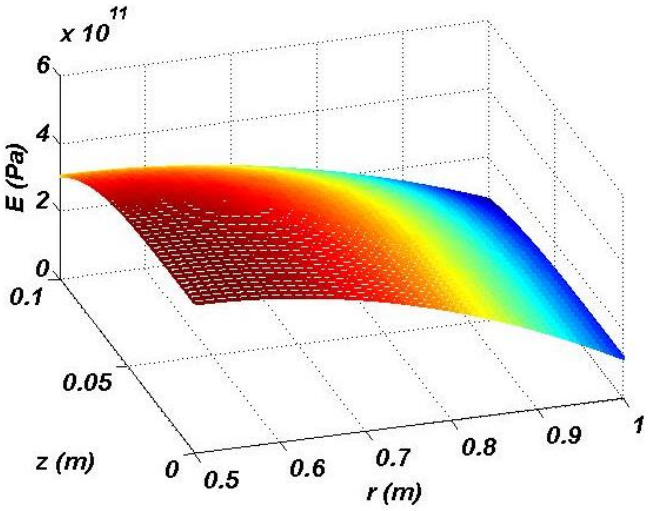

Fig. 3 Distribution of modulus of elasticity for n_r=2, n_z=3

The volume fractions in Eq. (1) reduce to the conventional 1D-FGMs for n_r=0. In this case, the material properties vary only through the thickness direction. The basic constituents of the 2D-FGM annular sector plate are presented in Table 1. For instance, the variation of a material property such as modulus of elasticity based on the mentioned approach, for the typical values of n_r=2, n_z=3 is shown in Fig. 3. It should be noted that Poisson's ratio is assumed to be constant through the body. This assumption is reasonable because of the small differences between the Poisson's ratios of basic materials.

In the absence of body forces, the equilibrium equations of 2D-FGM annular sector plates in cylindrical coordinates can be written as follows (Sadd 2005)

$$\frac{\partial \sigma_{rr}}{\partial r}+\frac{\partial \sigma_{r\theta}}{r\partial \theta}+\frac{\partial \sigma_{rz}}{\partial z}+\frac{\sigma_{rr}-\sigma_{\theta\theta}}{r}=\rho(r,z)\frac{\partial^2 u}{\partial t^2} \tag{3-1}$$

$$\frac{\partial \sigma_{r\theta}}{\partial r}+\frac{\partial \sigma_{\theta\theta}}{r\partial \theta}+\frac{\partial \sigma_{\theta z}}{\partial z}+\frac{2\sigma_{r\theta}}{r}=\rho(r,z)\frac{\partial^2 v}{\partial t^2} \tag{3-2}$$

$$\frac{\partial \sigma_{rz}}{\partial r}+\frac{\partial \sigma_{\theta z}}{r\partial \theta}+\frac{\partial \sigma_{zz}}{\partial z}+\frac{\sigma_{rz}}{r}=\rho(r,z)\frac{\partial^2 w}{\partial t^2} \tag{3-3}$$

where ρ is the mass density which depends on r and z coordinates. u, v, and w are the displacement components along the r, θ and z axes, respectively.

The stress- strain relations of linear elasticity from the Hook's law in terms of the modulus of elasticity E and Poisson's ratio v in cylindrical coordinates are as follow

$$[\sigma]_{r,\theta,z} = [D][\varepsilon]_{r,\theta,z,} \quad [\sigma]_{r,\theta,z} = \begin{bmatrix} \sigma_{rr} \\ \sigma_{\theta\theta} \\ \sigma_{zz} \\ \sigma_{\theta z} \\ \sigma_{rz} \\ \sigma_{r\theta} \end{bmatrix}, \quad [\varepsilon]_{r,\theta,z} = \begin{bmatrix} \varepsilon_{rr} \\ \varepsilon_{\theta\theta} \\ \varepsilon_{zz} \\ \gamma_{\theta z} \\ \gamma_{rz} \\ \gamma_{r\theta} \end{bmatrix} \tag{4}$$

$$[D] = \frac{E(r,z)(1-\nu)}{(1+\nu)(1-2\nu)} \begin{pmatrix} 1 & \frac{\nu}{1-\nu} & \frac{\nu}{1-\nu} & 0 & 0 & 0 \\ \frac{\nu}{1-\nu} & 1 & \frac{\nu}{1-\nu} & 0 & 0 & 0 \\ \frac{\nu}{1-\nu} & \frac{\nu}{1-\nu} & 1 & 0 & 0 & 0 \\ 0 & 0 & 0 & \frac{1-2\nu}{2(1-\nu)} & 0 & 0 \\ 0 & 0 & 0 & 0 & \frac{1-2\nu}{2(1-\nu)} & 0 \\ 0 & 0 & 0 & 0 & 0 & \frac{1-2\nu}{2(1-\nu)} \end{pmatrix} \tag{5}$$

It should be noted that E varies through the r and z directions and ν is assumed to be constant.

The problem is solved in the rectangular Cartesian coordinates system and then the displacement and stress components transformed into the cylindrical coordinates system using the following relations.

$$u = U\cos\theta + V\sin\theta \tag{6-1}$$

$$v = U\cos\theta - V\sin\theta \tag{6-2}$$

$$[\sigma]_{r,\theta,z} = \begin{pmatrix} \cos^2\theta & \sin^2\theta & 0 & 0 & 0 & 2\sin\theta\cos\theta \\ \sin^2\theta & \cos^2\theta & 0 & 0 & 0 & -2\sin\theta\cos\theta \\ 0 & 0 & 1 & 0 & 0 & 0 \\ 0 & 0 & 0 & \cos\theta & -\sin\theta & 0 \\ 0 & 0 & 0 & \sin\theta & \cos\theta & 0 \\ -\cos\theta\sin\theta & \cos\theta\sin\theta & & 0 & 0 & \cos^2\theta - \sin^2\theta \end{pmatrix} [\sigma]_{x,y,z} \tag{6-3}$$

where U and V are the displacement components in rectangular Cartesian coordinate system. $[\sigma]_{x,y,z}$ is the stress tensor in rectangular Cartesian coordinate systems.

So, the equilibrium equations in terms of rectangular Cartesian coordinates system are as following (Sadd 2005)

$$\frac{\partial \sigma_{xx}}{\partial x}+\frac{\partial \sigma_{xy}}{\partial y}+\frac{\partial \sigma_{zx}}{\partial z}=\rho(r(x,y),z)\frac{\partial^2 U}{\partial t^2} \tag{7-1}$$

$$\frac{\partial \sigma_{xy}}{\partial x}+\frac{\partial \sigma_{yy}}{\partial y}+\frac{\partial \sigma_{yz}}{\partial z}=\rho(r(x,y),z)\frac{\partial^2 V}{\partial t^2} \tag{7-2}$$

$$\frac{\partial \sigma_{zx}}{\partial x}+\frac{\partial \sigma_{yz}}{\partial y}+\frac{\partial \sigma_{zz}}{\partial z}=\rho(r(x,y),z)\frac{\partial^2 w}{\partial t^2} \tag{7-3}$$

where $r=\left(x^2+y^2\right)^{\frac{1}{2}}$.

The stress- strain relations of linear elasticity in Cartesian coordinates are as following

$$[\sigma]_{x,y,z}=[D][\varepsilon],\quad [\sigma]_{x,y,z}=\begin{bmatrix}\sigma_{xx}\\ \sigma_{yy}\\ \sigma_{zz}\\ \sigma_{yz}\\ \sigma_{xz}\\ \sigma_{xy}\end{bmatrix},\quad [\varepsilon]_{x,y,z}=\begin{bmatrix}\varepsilon_{xx}\\ \varepsilon_{yy}\\ \varepsilon_{zz}\\ \gamma_{yz}\\ \gamma_{xz}\\ \gamma_{xy}\end{bmatrix} \tag{8}$$

So, the strain-displacement relations of the infinitesimal theory of elasticity in the rectangular Cartesian coordinates are

$$[\varepsilon]=[d][q],\quad [d]=\begin{pmatrix}\frac{\partial}{\partial x} & 0 & 0\\ 0 & \frac{\partial}{\partial y} & 0\\ 0 & 0 & \frac{\partial}{\partial z}\\ 0 & \frac{\partial}{\partial z} & \frac{\partial}{\partial y}\\ \frac{\partial}{\partial z} & 0 & \frac{\partial}{\partial x}\\ \frac{\partial}{\partial y} & \frac{\partial}{\partial x} & 0\end{pmatrix},\quad [q]=\begin{bmatrix}U\\ V\\ w\end{bmatrix} \tag{9}$$

3. Graded finite element modeling

Consider a three dimensional 8-node linear brick shape element in the rectangular Cartesian coordinates. Nodal coordinates are known in the global *xyz*- coordinates. Using the finite element approximation to the displacement field, the displacement component are approximated by shape function *N*, as

$$[q]^{(e)} = [N]^{(e)}[\delta]^{(e)}, \quad [\delta]^{(e)} = \begin{pmatrix} U_1 \\ V_1 \\ w_1 \\ . \\ . \\ . \\ U_8 \\ V_8 \\ w_8 \end{pmatrix} \tag{10}$$

where $[\delta]^{(e)}$ is the nodal displacement vector in rectangular Cartesian coordinates, and shape function matrix is as follows

$$[N]^{(e)} = \begin{bmatrix} N_1 & 0 & 0 & N_2 & 0 & 0 & N_3 & 0 & 0 & N_4 & 0 & 0 & N_5 & 0 & 0 & N_6 & 0 & 0 & N_7 & 0 & 0 & N_8 & 0 & 0 \\ 0 & N_1 & 0 & 0 & N_2 & 0 & 0 & N_3 & 0 & 0 & N_4 & 0 & 0 & N_5 & 0 & 0 & N_6 & 0 & 0 & N_7 & 0 & 0 & N_8 & 0 \\ 0 & 0 & N_1 & 0 & 0 & N_2 & 0 & 0 & N_3 & 0 & 0 & N_4 & 0 & 0 & N_5 & 0 & 0 & N_6 & 0 & 0 & N_7 & 0 & 0 & N_8 \end{bmatrix} \tag{11}$$

where N_i, i=1,2,…,8 are the shape functions of 8-node linear brick element. The components of matrix $[N]^{(e)}$ are given in the appendix A.

To model the problem, Graded Finite Element Method is used (Santare and Lambros 2000, Kim and Paulino 2002, Santare *et al*. 2003, Zhang and Paulino 2007, Asgari and Akhlaghi 2009, 2010, 2011, Asemi *et al*. 2012). This method employs the same shape functions to interpolate the unknown displacements, the geometry, and the material parameters. This approach effectively represents the material variation at the element level and results in smooth solution transition across the element boundaries. This gives more accurate results than dividing the solution domain into homogenous elements. Therefore, the material property at the element level is interpolated as follows

$$P = \sum_{i=1}^{8} P_i N_i \tag{12}$$

where P_i is the material property corresponding to node i.

Substituting (10) in (9) gives the strain matrix of element (e) as

$$[\varepsilon]^{(e)} = [B]^{(e)}[\delta]^{(e)} \tag{13}$$

where $[B]^{(e)}=[d][N]^{(e)}$ and is given in the Appendix A.

The finite element model can be derived using Rayleigh Ritz energy formulation. The details of this method could be found in different textbooks (Eslami 2003, Zienkiewicz and Taylor 2005).

By applying this method to the governing equations, the stiffness, mass and force element matrices in Cartesian coordinate system are as follows

$$[K]^{(e)} = \int_{V_{(e)}} [B]^T [D][B] dV \tag{14}$$

$$[M]^{(e)} = \int_{V_{(e)}} \rho [N]^T [N] dV \tag{15}$$

$$[F]^{(e)} = \int_{A_{(e)}} [N]^T \{p(t)\} dA, \quad \{p(t)\} = \begin{Bmatrix} 0 \\ 0 \\ p_z(t) \end{Bmatrix} \tag{16}$$

Using 8-point Guass quadrature rule, mass and stiffness matrices are evaluated. In this regard, a transformation between Cartesian coordinate system into local coordinates system is used ($-1 \leq \xi, \eta, \zeta \leq 1$) (Zienkiewicz and Taylor 2005).

Now by assembling the element matrices, the global dynamic equilibrium equations for the 2D-FGM annular sector plate can be obtained as

$$[M]\{\ddot{\delta}\} + [K]\{\delta\} = \{F\} \tag{17}$$

The essential boundary conditions are as

For fully clamped plates (CCCC)

$$u,v,w\,(r,0,z) = u,v,w\,(r,\theta_{max},z) = u,v,w\,(a,\theta,z) = u,v,w\,(b,\theta,z) = 0 \tag{18}$$

For plates with clamped edges at θ=0and $\theta=\theta_{\max}$ (CFCF)

$$u,v,w\,(r,0,z) = u,v,w\,(r,\theta_{max},z) = 0 \tag{19}$$

For plates with clamp edge at $r=a$ (FCFF)

$$u,v,w\,(a,\theta,z) = 0 \tag{20}$$

For plates with clamp edge at $r=b$ (FFFC)

$$u,v,w\,(b,\theta,z) = 0 \tag{21}$$

Once the finite element equilibrium equation is established, different numerical methods can be employed to solve Eq. (17) in space and time domains. To solve the equilibrium equation, the Newmark direct integration method (Eslami 2003) is used. Newmark integration parameters (Eslami 2003) are taken as: $\gamma = \frac{1}{2}$ and $\beta = \frac{1}{4}$, which lead to a constant average acceleration. This choice of parameters corresponds to a trapezoidal rule which is unconditionally stable in linear

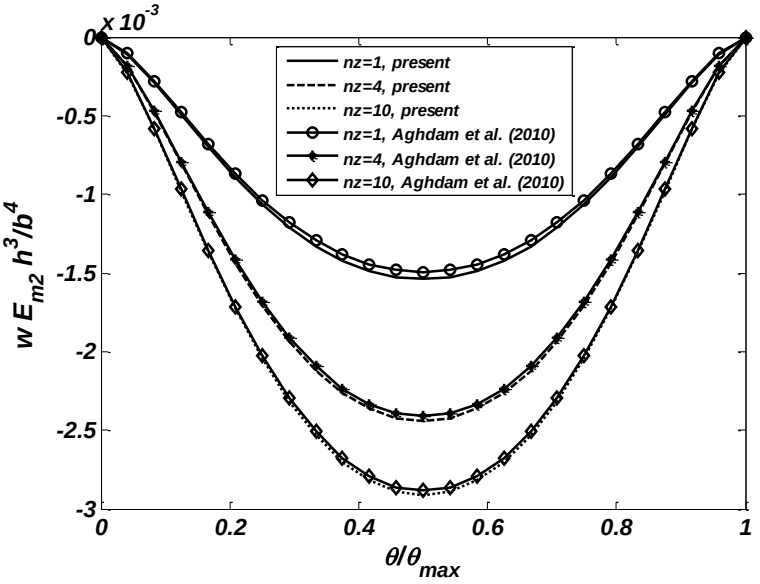

Fig. 4 Non-dimensional transverse displacement through the $\left(\frac{a+b}{2},\theta,\frac{h}{2}\right)$ compared with Aghdam *et al*. (2010)

analyzes. Moreover, to achieve convergent results, the time step is taken as 2*e*-6 (s). It should be noted that the problem generally is solved in rectangular Cartesian coordinates system followed by a transformation of the displacements and stresses components into the cylindrical coordinates.

4. Results and discussions

4.1 Validation

The present solution can be validated using data of a 1D-FGM fully clamped plate under the same loading that were previously presented (Aghdam *et al*. 2010). So, we consider the parameters as n_r=0, a=3, b=5, h=0.3, θ=45°, E_{m1}=70 GPa, E_{m2}=380 GPa, P=1 Pa and υ=0.3. The non-dimensional transverse displacement through the centerline $\left(\frac{a+b}{2},\theta,\frac{h}{2}\right)$ for different power law exponent n_z is considered here, and the obtained results are compared with the published data. Fig. 4 shows good agreement between these results.

4.2 Numerical results

4.2.1 Static analysis

Consider a 2D-FGM annular sector plate with inner radii a=0.5 m, outer radii b=1 m, sector angle θ=60° and thicknesses h=0.1 m. The plate is all-round clamped and subjected to a uniform static load on its top surface. Constituent materials are two distinct ceramics and two distinct

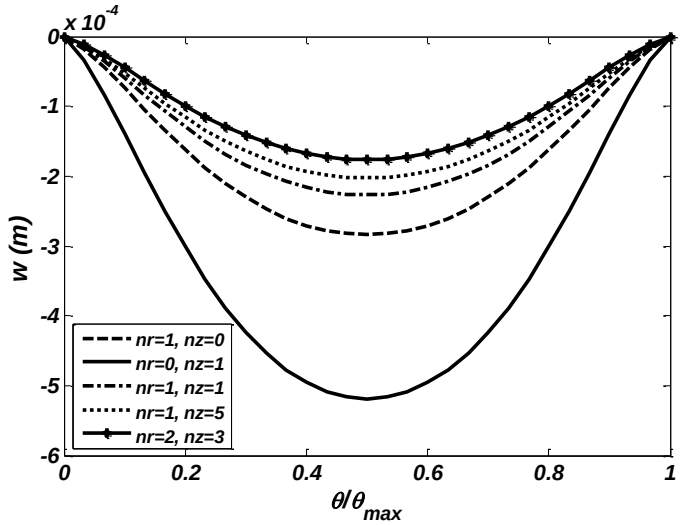

Fig. 5 Transverse displacement distribution through $\left(\frac{a+b}{2},\theta,\frac{h}{2}\right)$ for different power law exponents

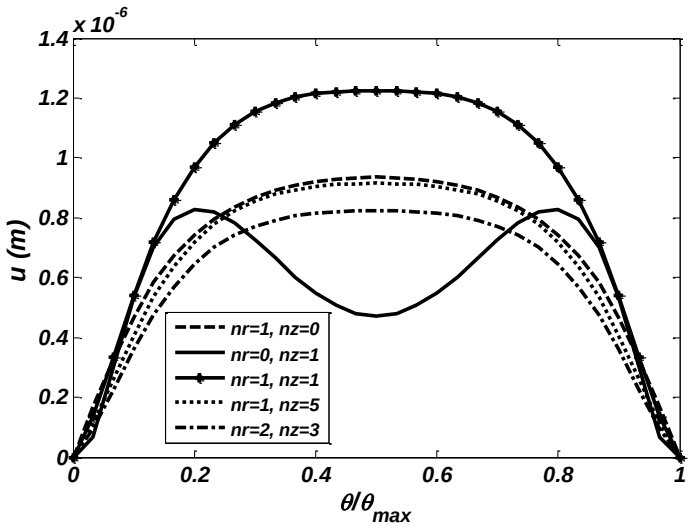

Fig. 6 Radial displacement distribution through $\left(\frac{a+b}{2},\theta,\frac{h}{2}\right)$ for different power law exponents

metals described in Table 1. The static pressures and Poisson's ratio are taken as constant values: P=20 MPa and $\upsilon = 0.3$.

Figs. 5, 6 and 7 show the distribution of transverse, radial and hoop displacements at centerline $\left(\frac{a+b}{2},\theta,\frac{h}{2}\right)$ for different values of power law exponents. Fig. 5 denotes that by increasing the power law exponent n_z (n_r=1), the transverse displacement decreases. This is because of increasing

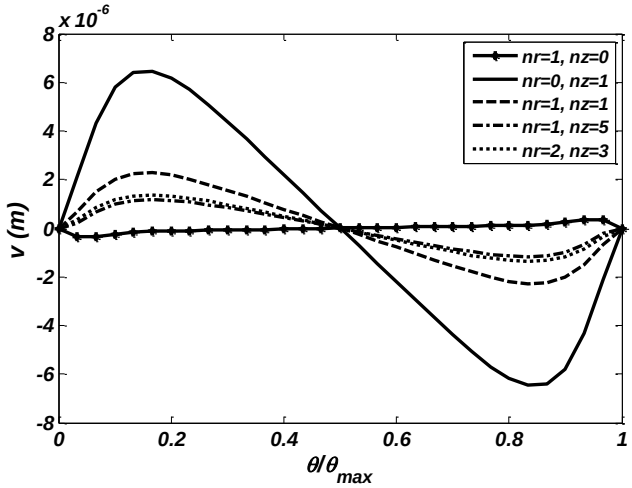

Fig. 7 Hoop displacement distribution through $\left(\frac{a+b}{2},\theta,\frac{h}{2}\right)$ for different power law exponents

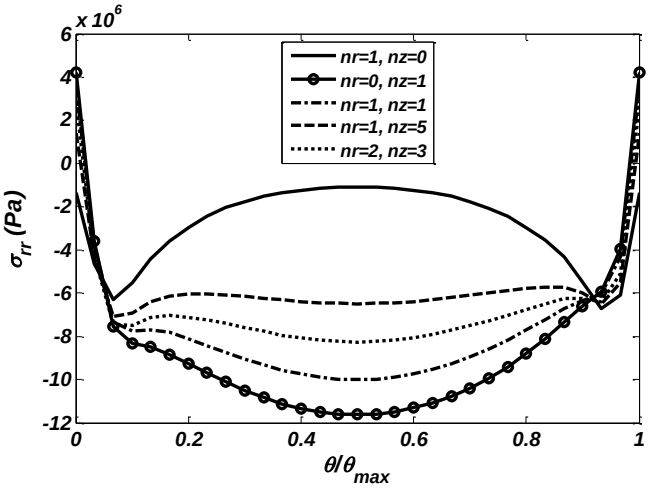

Fig. 8 Radial stress distribution through $\left(\frac{a+b}{2},\theta,\frac{h}{2}\right)$ for different power law exponents

the volume fraction of first ceramic and subsequently increasing the overall stiffness of the plate. It is seen from Fig. 5 that the minimum value of transverse displacement belongs to n_r=2, n_r=3 and its maximum value is obtained for the power law exponents n_r=0, n_z=1 which is for the transversely 1D-FGMs. Fig. 6 denotes that the general form of the radial displacement for n_r=0, n_z=1, i.e., for conventional transversely 1D-FGM sector plates differs from the obtained radial displacements corresponds to 2D-FGMs. Fig. 7 shows that the distribution of hoop displacement is asymmetrical about centerline $\left(r,\frac{\theta_{max}}{2},\frac{h}{2}\right)$.

Figs. 8, 9, 10 and 11 show the distribution of radial, hoop and axial stresses and shear stress σ_{rz}

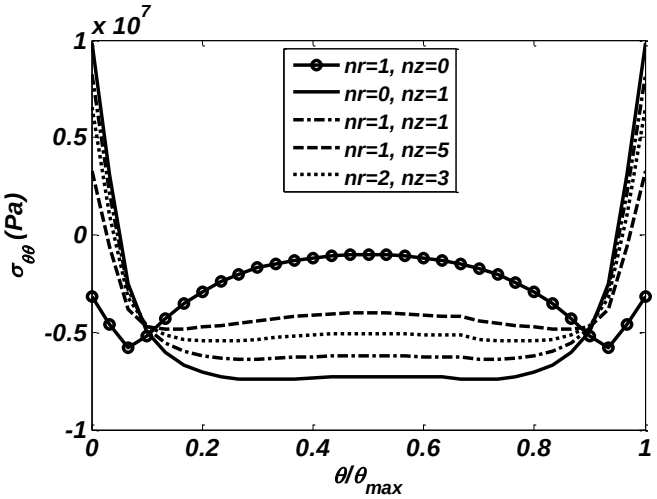

Fig. 9 Hoop stress distribution through $\left(\frac{a+b}{2},\theta,\frac{h}{2}\right)$ for different power law exponents

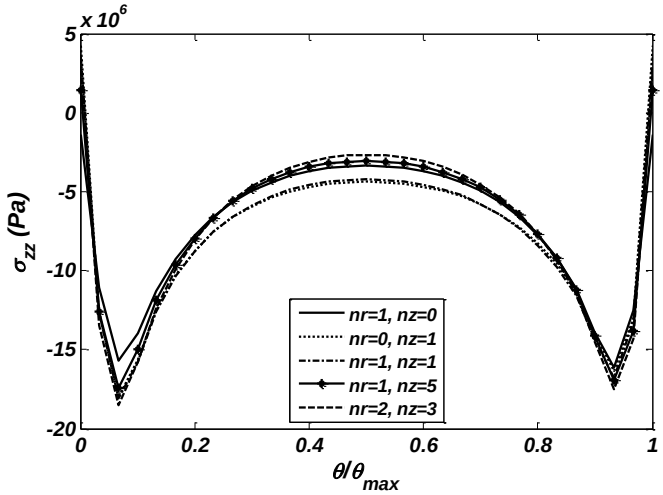

Fig. 10 Axial stress distribution through $\left(\frac{a+b}{2},\theta,\frac{h}{2}\right)$ for different power law exponents

at centerline $\left(\frac{a+b}{2},\theta,\frac{h}{2}\right)$ for different values of power law exponents, respectively. Figs. 8 and 9 show that the nature of radial and hoop stress is mainly compressive and its maximum value belongs to the power law exponents n_r=0, n_z=1, in which the material properties vary only through the thickness direction. Fig. 10 shows that the distribution of the axial stress does not change considerably with the power law exponents. Fig. 11 shows that the shear stress σ_{rz} is mainly tensile and its maximum and minimum values belong to the power law exponents n_r=0, n_z=1 and n_r=1, n_z=0 which are respectively for transversely and radially 1D-FGMs. As it can be seen from the results, the distribution of stresses has continuous variations due to using graded elements.

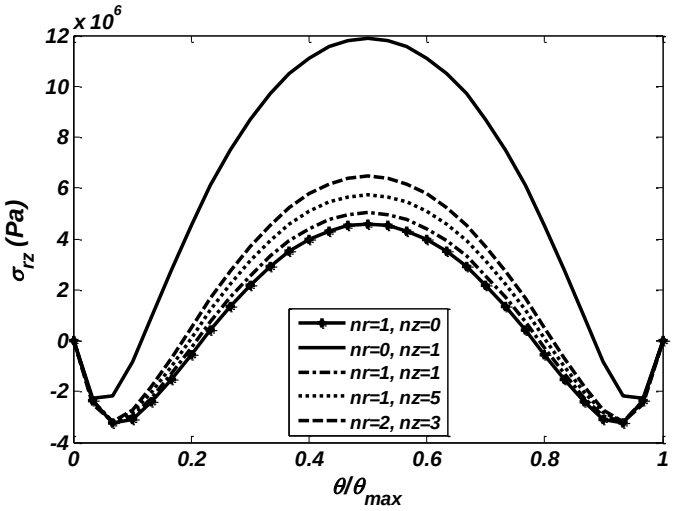

Fig. 11 Shear stress distribution σ_{rz} through $\left(\frac{a+b}{2},\theta,\frac{h}{2}\right)$ for different power law exponents

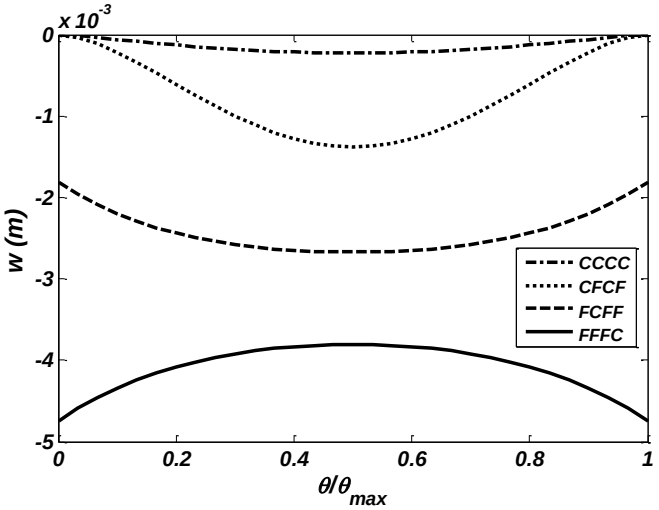

Fig. 12 Transverse displacement distribution through $\left(\frac{a+b}{2},\theta,\frac{h}{2}\right)$ for different boundary conditions and power law exponents n_r=n_z=1

Figs. 12 and 13 show the distribution of transverse and radial displacements at centerline $\left(\frac{a+b}{2},\theta,\frac{h}{2}\right)$ for power law exponents n_r=n_z=1 and different boundary conditions. As it can be seen from these figures, the fully clamped plate has minimum values of displacements and the plate with clamped edge at r=b has maximum values of displacements. These results show that the present solution has a high compatibility to model the 2D-FGM annular sector plates under different boundary conditions.

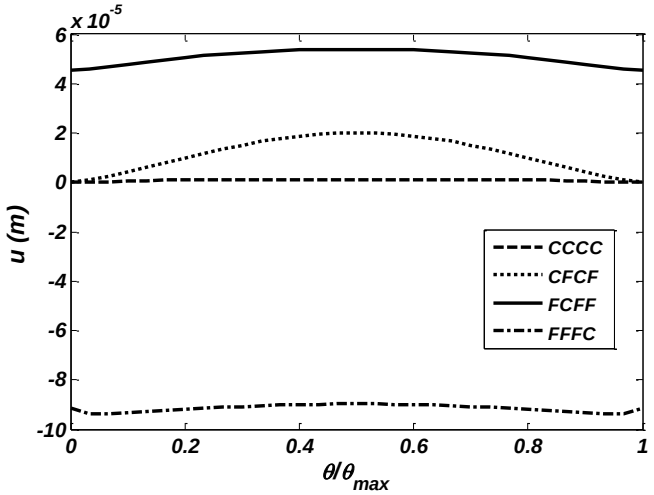

Fig. 13 Radial displacement distribution through $\left(\frac{a+b}{2},\theta,\frac{h}{2}\right)$ for different boundary conditions and power law exponents n_r=n_z=1

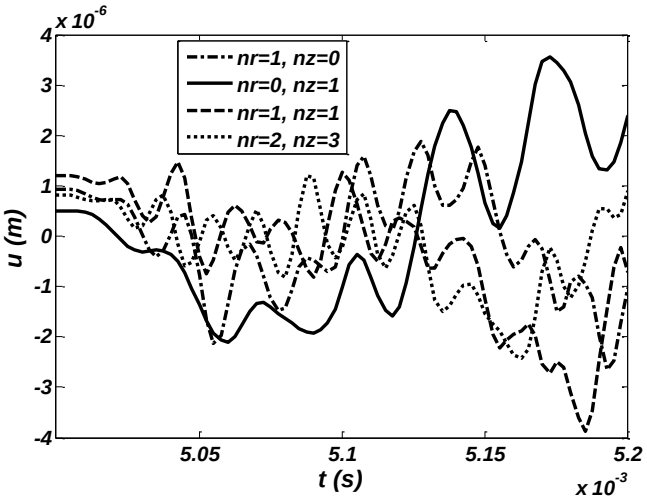

Fig. 14 Time history of radial displacement at $\left(\frac{a+b}{2},\frac{\theta_{max}}{2},\frac{h}{2}\right)$ for different power law exponents

4.2.2 Dynamic analysis

Consider the 2D-FGM sector plate of the previous section. The plate is fully clamped and subjected to an dynamic loading on its top surface. The loading function equation is assumed as:

$$P(t)=\begin{cases}P_0 t & t\le 0.005\ (s)\\ 0 & t>0.005\ (s)\end{cases}$$

where P_0 is assumed as 4 GPa/s. The plate is excited by unloading in t=0.005 (s). It is obvious that after the unloading, a transient vibration which is affected by the wave propagation, reflection and

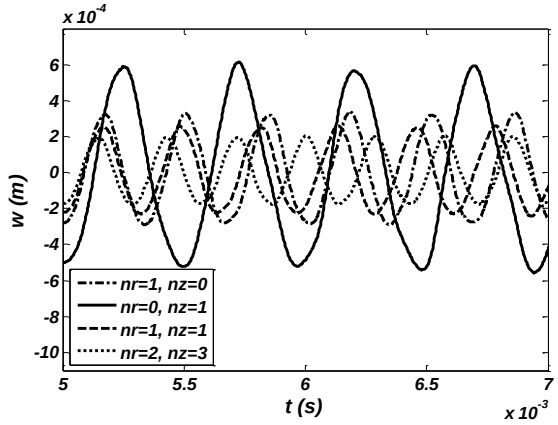

Fig. 15 Time history of transverse displacement at $\left(\frac{a+b}{2}, \frac{\theta_{max}}{2}, \frac{h}{2}\right)$ for different power law exponents

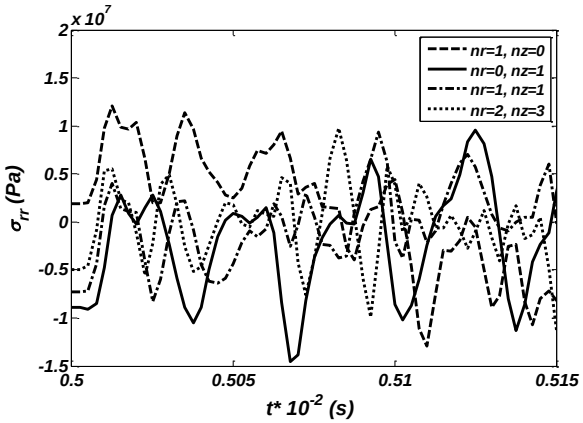

Fig. 16 Time history of radial stress at $\left(\frac{a+b}{2}, \frac{\theta_{max}}{2}, \frac{h}{2}\right)$ for different power law exponents

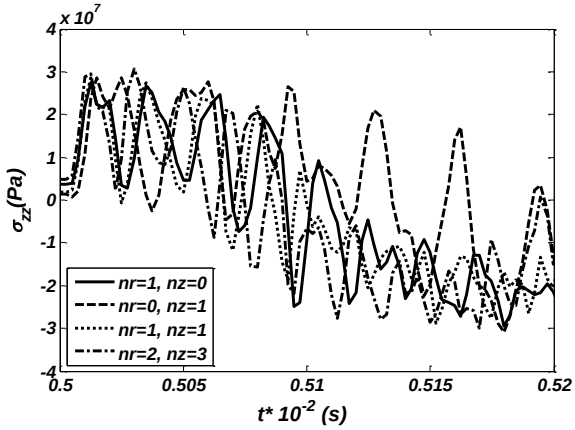

Fig. 17 Time history of axial stress at $\left(\frac{a+b}{2}, \frac{\theta_{max}}{2}, \frac{h}{2}\right)$ for different power law exponents

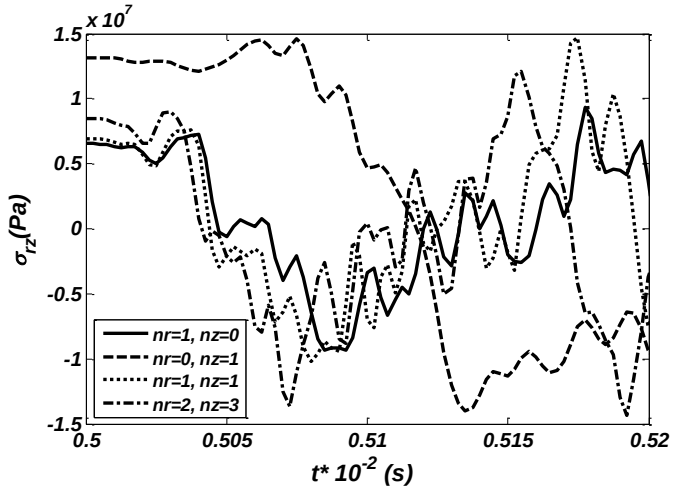

Fig. 18 Time history of shear stress σ_{rz} at $\left(\frac{a+b}{2}, \frac{\theta_{max}}{2}, \frac{h}{2}\right)$ for different power law exponents

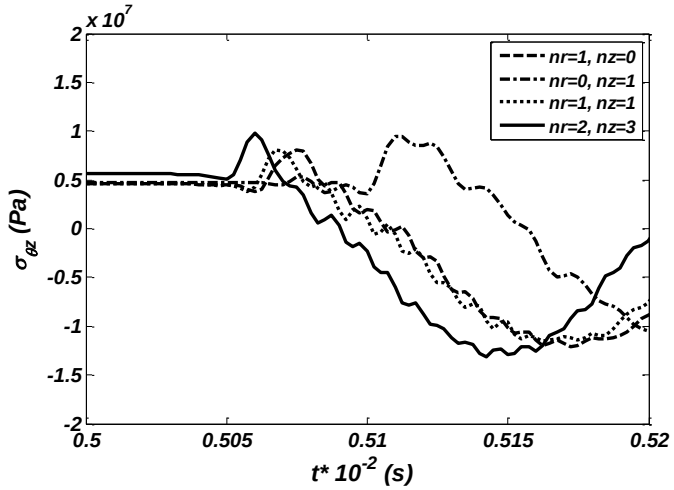

Fig. 19 Time history of shear stress $\sigma_{\theta z}$ at $\left(\frac{a+b}{2}, \frac{\theta_{max}}{2}, \frac{h}{2}\right)$ for different power law exponents

interference would be occurred. The results for different values of the power law exponents are presented and discussed as following.

Figs. 14 and 15 show the time histories of radial and transverse displacements of the center point of the plate after the unloading for different values of the power law exponents, respectively. Fig. 15 shows that by increasing the power law exponent n_z (n_r=1), amplitude of vibration decreases. Moreover, maximum amplitude of vibration belongs to the plate with the power law exponents n_r=0, n_z=1. Figs. 16, 17, 18 and 19 show the time histories of radial and axial stresses, shear stress σ_{rz} and shear stress $\sigma_{\theta z}$ of the center point of the plate after the unloading for different values of the power law exponents, respectively. Results denote that the time history of stresses is strongly affected by the power law exponents.

6. Conclusions

Static and dynamic analysis of two dimensional functionally graded annular sector plate based on three dimensional theory of elasticity is considered. Material properties vary through both the radial and axial directions. The Graded Finite Element Method and Rayleigh-Ritz energy formulation are applied. The proposed method is validated by the result of a fully clamped 1D-FGM plate under the same loading which is extracted from published literature. The comparisons between the results show that the present method has a good compatibility with the existing results. The obtained results represent that mechanical stress distribution can be modified to a required manner by selecting an appropriate volume fraction profiles in two directions and this gives designers a powerful tool for flexible designing of structures under multifunctional requirements. Also results demonstrate that using graded elements provide smoother and more accurate results than homogeneous elements for modeling the dynamic problems.

References

Aghdam, M.M., Shahmansouri, N. and Mohammadi, M. (2010), "Extended Kantorovich method for rstatic analysis of moderately thick functionally graded sector plates", *Math. Comput. Simul*., DOI: 10.1016/j.matcom.2010.07.029

Asemi, K., Salehi, M. and Akhlaghi, M. (2010), "Dynamic analysis of a functionally graded thick truncated cone with finite length", *Int. J. Mech. Mater. Des*., **6**, 367-378.

Asemi, K., Akhlaghi, M., Salehi, M. and Hosseini Zad, S.K. (2011), "Analysis of functionally graded thick truncated cone with finite length under hydrostatic internal pressure", *Arch. Appl. Mech*., **81**, 1063-1074.

Asemi, K., Salehi, M. and Akhlaghi, M. (2011), "Elastic solution of a two-dimensional functionally graded thick truncated cone with finite length under hydrostatic combined loads", *Acta Mech*., **217**(1-2), 119-134.

Asemi, K., Akhlaghi, M. and Salehi, M. (2012), "Dynamic analysis of thick short FGM cylinders", *Meccanica*, **47**(6), 1441-1453.

Asgari, M., Akhlaghi, M. and Hosseini, S.M. (2009), "Dynamic analysis of two-dimensional functionally graded thick hollow cylinder with finite length under impact loading", *Acta Mech*., **208**(3-4), 163-180.

Asgari, M. and Akhlaghi, M. (2010), "Transient thermal stresses in two-dimensional functionally graded thick hollow cylinder with finite length", *Arch. Appl. Mech*., **80**(4), 353-376.

Asgari, M., Akhlaghi, M. (2011), "Natural frequency analysis of 2D-FGM thick hollow cylinder based on three-dimensional elasticity equations", *Eur. J. Mech. A/Solid*., **30**, 72-81

Behravan Rad, A. (2012), "Static response of 2-D functionally graded circular plate with gradient thickness and elastic foundations to compound loads", *Struct. Eng. Mech*., **44**(2), 139-161.

Behravan Rad, A. and Shariyat, M. (2013), "A three-dimensional elasticity solution for two-directional FGM annular plates with non-uniform elastic foundations subjected to normal and shear tractions", *Acta Mechanica Solida Sinica*, **26**(6), 671-690.

Bian, Z.G. and Wang, Y.H. (2013), "Axisymmetrical bending of single-and multi-span functionally graded hollow cylinders", *Struct. Eng. Mech*., **45**(3), 355-371.

Dong, C.Y. (2008), "Three-dimensional free vibration analysis of functionally graded annular plates using the Chebyshev-Ritz method", *Mater. Des*., **29**, 1518-1525

Eslami, M.R. (2003), *A First Course in Finite Element Analysis*, First Edition, Amirkabir University of Technology, Tehran publication Press.

Ghannad, M., Zamani Nejad, M., Rahimi, G.H. and Sabouri, H. (2012), "Elastic analysis of pressurized thick truncated conical shells made of functionally graded materials", *Struct. Eng. Mech.*, **43**(1), 105-126.

Goupee, A.J. and Vel, S.S. (2006), "Two-dimensional optimization of material composition of functionally graded materials using mesh less analyses and a genetic algorithm", *Comput. Meth. Appl. Mech. Eng.*, **195**(44-47), 5926-5948.

Jodaei, A., Jalal, M. and Yas, M.H. (2012), "Free vibration analysis of functionally graded annular plates by state-space based differential quadrature method and comparative modeling by ANN", *Compos. Part B*, **43**, 340-353

Kim, J.H. and Paulino, G.H. (2002), "Isoparametric graded finite elements for nonhomogeneous isotropic and orthotropic materials", *J. Appl. Mech.*, **69**(4), 502-514.

Lei, Z. and Zheng, Z. (2009), "Exact solution for axisymmetric bending of functionally graded circular plate", *Tsinghua Sci. Technol.*, **14**, 64-68.

Li, X.Y., Ding, H.J. and Chen, W.Q. (2006), "Pure bending of simply supported circular plate of transversely isotropic functionally graded material", *J. Zhejiang Univ. Sci. A*, **7**, 1324-1328.

Li, X.Y., Ding, H.J. and Chen, W.Q. (2008), "Elasticity solutions for a transversely isotropic functionally graded circular plate subject to an axisymmetric transverse load qr^k", *Int. J. Solid. Struct.*, **45**, 191-210.

Li, X.Y., Ding, H.J. and Chen, W.Q. (2008), "Axisymmetric elasticity solutions for a uniformly loaded annular plate of transversely isotropic functionally graded materials", *Acta Mech.*, **196**, 139-159.

Lu, C.F., Chen, W.Q., Xu, R.Q. and Lim, C.W. (2008), "Semi-analytical elasticity solutions for bi-directional functionally graded beams", *Int. J. Solid. Struct.*, **45**(1), 258-275.

Nemat-Alla, M. (2009), "Reduction of thermal stresses by composition optimization of two-dimensional functionally graded materials", *Acta Mech.*, **208**(3-4), 147-161.

Nie, G. and Zhong, Z. (2007), "Axisymmetric bending of two-directionall functionally graded circular and annular plates", *Acta Mechanica Solida Sinica*, **20**(4), 289-295.

Nie, G.J. and Zhong, Z. (2008), "Vibration analysis of functionally graded annular sectorial plates with simply supported radial edges", *Compos. Struct.*, **84**, 167-176.

Nosier, A. and Fallah, F. (2008), **"**Reformulation of Mindlin-Reissner governing equations of functionally graded circular plates", *Acta Mech.*, **198**, 209-233.

Rahmati Nezhad, Y., Asemi, K. and Akhlaghi, M. (2011), "Transient solution of temperature field in functionally graded hollow cylinder with finite length using multi layered approach", *Int. J. Mech. Mater. Des.*, **7**, 71-82.

Reddy, J.N., Wang, C.M. and Kitipornchai, S. (1999), "Axisymmetric bending of functionally graded circular and annular plates", *Eur. J. Mech. A/Solid.*, **18**, 185-199.

Sadd, M.H. (2005), *Elasticity Theory, Applications, and Numerics*, Elsevier Butterworth-Heinemann, Burlington, MA.

Saidi, A.R., Hasani Baferani, A. and Jomehzadeh, E. (2011), "Benchmark solution for free vibration of functionally graded moderately thick annular sector plates", *Acta Mech.*, **219**, 309-335.

Santare, M.H. and Lambros, J. (2000), "Use of Graded Finite Elements to Model the Behavior of Nonhomogeneous Materials", *J. Appl. Mech.*, **67**(4), 819-22.

Santare, M.H., Thamburaj, P. and Gazonas, G.A. (2003), "The use of graded finite elements in the study of elastic wave propagation in continuously nonhomogeneous materials", *Int. J. Solid. Struct.*, **40**(21), 5621-5634.

Sburlati, R. and Bardella, L. (2011), "Three-dimensional elastic solutions for functionally graded circular plates", *Eur. J. Mech. A/Solid.*, **30**, 219-235.

Shariyat, M. and Alipour, M.M. (2011), "Differential transform vibration and modal stress analyses of circular plates made of two-directional functionally graded materials resting on elastic foundations", *Arch. Appl. Mech.*, **81**(9), 1289-1306.

Sobhani Aragh, B. and Hedayati, H. (2012), "Static response and free vibration of two-dimensional functionally graded metal/ceramic open cylindrical shells under various boundary conditions", *Acta Mech.*, **223**(2), 309-330.

Tahouneh, V. and Yas M.H. (2012), "3-D free vibration analysis of thick functionally graded annular sector

plates on Pasternak elastic foundation via 2-D differential quadrature method", *Acta Mechanica*, **223**(9), 1879-1897.

Tajeddini, V., Ohadi, A. and Sadighi, M. (2011), "Three-dimensional free vibration of variable thickness thick circular and annular isotropic and functionally graded plates on Pasternak foundation", *Int. J. Mech. Sci*., **53**, 300-308

Yas, M.H., Sobhani Aragh, B. and Heshmati, M. (2011), "Three-dimensional free vibration analysis of functionally graded fiber reinforced cylindrical panels using differential quadrature method", *Struct. Eng. Mech*., **37**(5), 529-542.

Yun, W., Rongqiao, X. and Haojiang, D. (2010), "Three-dimensional solution of axisymmetric bending of functionally graded circular plates", *Compos. Struct*., **92**, 1683-1693.

Zhang, Z. and Paulino, G.H. (2007), "Wave propagation and dynamic analysis of smoothly graded heterogeneous continua using graded finite elements", *Int. J. Solid. Struct*., **44**(11-12), 3601-3626.

Zienkiewicz, O.C. and Taylor, R.L. (2005), *The Finite Element Method for Solid and Structural Mechanics*, Sixth Edition, Elsevier Butterworth-Heinemann, Oxford.

Appendix

The shape functions for local coordinates ($-1 \leq \xi, \eta, \zeta \leq 1$) are as following

$$N_1 = \frac{1}{8}(1-\xi)(1-\eta)(1-\zeta) \tag{A.1}$$

$$N_2 = \frac{1}{8}(1+\xi)(1-\eta)(1-\zeta) \tag{A.2}$$

$$N_3 = \frac{1}{8}(1+\xi)(1+\eta)(1-\zeta) \tag{A.3}$$

$$N_4 = \frac{1}{8}(1-\xi)(1+\eta)(1-\zeta) \tag{A.4}$$

$$N_5 = \frac{1}{8}(1-\xi)(1-\eta)(1+\zeta) \tag{A.5}$$

$$N_6 = \frac{1}{8}(1+\xi)(1-\eta)(1+\zeta) \tag{A.6}$$

$$N_7 = \frac{1}{8}(1+\xi)(1+\eta)(1+\zeta) \tag{A.7}$$

$$N_8 = \frac{1}{8}(1-\xi)(1+\eta)(1+\zeta) \tag{A.8}$$

The coordinate transformation law between two coordinate systems can be described in terms of the shape functions as (Zienkiewicz and Taylor 2005)

$$x(\xi,\eta,\zeta) = \sum_{i=1}^{8} N_i x_i \tag{A.9}$$

$$y(\xi,\eta,\zeta) = \sum_{i=1}^{8} N_i y_i \tag{A.10}$$

$$z(\xi,\eta,\zeta)=\sum_{i=1}^{8}N_i z_i \tag{A.11}$$

where x_i, y_i and z_i are nodal coordinates.

Matrix B is as following

$$B=\begin{pmatrix}
\frac{\partial N_1}{\partial x} & 0 & 0 & \frac{\partial N_2}{\partial x} & 0 & 0 & \dots & \frac{\partial N_8}{\partial x} & 0 & 0\\
0 & \frac{\partial N_1}{\partial y} & 0 & 0 & \frac{\partial N_2}{\partial y} & 0 & \dots & 0 & \frac{\partial N_8}{\partial y} & 0\\
0 & 0 & \frac{\partial N_1}{\partial z} & 0 & 0 & \frac{\partial N_2}{\partial z} & \dots & 0 & 0 & \frac{\partial N_8}{\partial z}\\
0 & \frac{\partial N_1}{\partial z} & \frac{\partial N_1}{\partial y} & 0 & \frac{\partial N_2}{\partial z} & \frac{\partial N_2}{\partial y} & \dots & 0 & \frac{\partial N_8}{\partial z} & \frac{\partial N_8}{\partial y}\\
\frac{\partial N_1}{\partial z} & 0 & \frac{\partial N_1}{\partial x} & \frac{\partial N_2}{\partial z} & 0 & \frac{\partial N_2}{\partial x} & \dots & \frac{\partial N_8}{\partial z} & 0 & \frac{\partial N_8}{\partial x}\\
\frac{\partial N_1}{\partial y} & \frac{\partial N_1}{\partial x} & 0 & \frac{\partial N_2}{\partial y} & \frac{\partial N_2}{\partial x} & 0 & \dots & \frac{\partial N_8}{\partial y} & \frac{\partial N_8}{\partial x} & 0
\end{pmatrix} \tag{A.12}$$

Matrix B in local coordinates is calculated as following

$$\hat{B}=J^{-1}\bar{B} \tag{A.13}$$

$$B(\xi,\eta,\zeta)=\begin{pmatrix}
\hat{B}(1,1) & 0 & 0 & \hat{B}(1,2) & 0 & 0 & \dots & \hat{B}(1,8) & 0 & 0\\
0 & \hat{B}(2,1) & 0 & 0 & \hat{B}(2,2) & 0 & \dots & 0 & \hat{B}(2,8) & 0\\
0 & 0 & \hat{B}(3,1) & 0 & 0 & \hat{B}(3,2) & \dots & 0 & 0 & \hat{B}(3,8)\\
0 & \hat{B}(3,1) & \hat{B}(2,1) & 0 & \hat{B}(3,2) & \hat{B}(2,2) & \dots & 0 & \hat{B}(3,8) & \hat{B}(2,8)\\
\hat{B}(3,1) & 0 & \hat{B}(1,1) & \hat{B}(3,2) & 0 & \hat{B}(1,2) & \dots & \hat{B}(3,8) & 0 & \hat{B}(1,8)\\
\hat{B}(2,1) & \hat{B}(1,1) & 0 & \hat{B}(2,2) & \hat{B}(1,2) & 0 & \dots & \hat{B}(2,8) & \hat{B}(1,8) & 0
\end{pmatrix} \tag{A.14}$$

where $\xi_i,\eta_i,\zeta_i=(\pm\frac{1}{\sqrt{3}},\pm\frac{1}{\sqrt{3}},\pm\frac{1}{\sqrt{3}})$ and the matrix J is the Jacobian matrix and is evaluated as follows

$$[J]=\left[\bar{B}\right]^{(e)}\begin{pmatrix} x_1 & y_1 & z_1 \\ x_2 & y_2 & z_2 \\ x_3 & y_3 & z_3 \\ x_4 & y_4 & z_4 \\ x_5 & y_5 & z_5 \\ x_6 & y_6 & z_6 \\ x_7 & y_7 & z_7 \\ x_8 & y_8 & z_8 \end{pmatrix} \tag{A.15}$$

where $[\bar{B}]^{(e)}$ is as

$$\left[\bar{B}\right]^{(e)}=\frac{1}{8}\begin{pmatrix} -(1-\eta)(1-\zeta) & (1-\eta)(1-\zeta) & (1+\eta)(1-\zeta) & -(1+\eta)(1-\zeta) & -(1-\eta)(1+\zeta) & (1-\eta)(1+\zeta) & (1+\eta)(1+\zeta)? & -(+\eta)(1+\zeta) \\ -(1-\xi)(1-\zeta) & -(1+\xi)(1-\zeta) & (1+\xi)(1-\zeta) & (1-\xi)(1-\zeta) & -(1-\xi)(1+\zeta) & -(1+\xi)(1+\zeta) & (1+\xi)(1+\zeta) & (1-\xi)(1+\zeta) \\ -(1-\xi)(1-\eta) & -(1+\xi)(1-\eta) & -(1+\xi)(1+\eta) & -(1-\xi)(1+\eta) & (1-\xi)(1-\eta) & (1+\xi)(1-\eta) & (1+\xi)(1+\eta) & (1-\xi)(1+\eta) \end{pmatrix} \tag{A.16}$$